Applied Energy 302 (2021) 117415

Contents lists available at ScienceDirect

Applied Energy

journal homepage: www.elsevier.com/locate/apenergy

A stochastic operational planning model for a zero emission building with emission compensation

Kasper Emil Thorvaldsen [a,*], Magnus Korpås [a], Karen Byskov Lindberg [a,b], Hossein Farahmand [a]

[a] Department of Electric Power Engineering, Norwegian University of Science and Technology, Norway
[b] SINTEF Community, Oslo, Norway

ARTICLE INFO

Keywords:
Operational planning
Stochastic dynamic programming
Grid interaction
Demand-side management
Hourly CO_{2eq}-intensity

ABSTRACT

The primary objective of Zero Emission Buildings (ZEBs) is to achieve net zero emission over the buildings' lifetime. To achieve this goal, accurate cost-effective emission compensation is needed during the operational phase. This paper presents a stochastic planning model comprising an emission inventory for the operation of ZEBs. The operational planning methodology uses stochastic dynamic programming (SDP) to analyze and represent the expected future cost curve (EFCC) for operation based on the electricity price and accumulated CO_{2eq}-inventory during the year. Failing to compensate for net zero emission makes the leftover amount subject to a penalty cost at the end of the year. This renders the overall problem multi-objective optimization including emission compensation and cost of operation. The model is applied to a case study of a Norwegian building, tested for a range of penalty costs for leftover CO_{2eq}-inventory. The results show that, for a ZEB, including emission compensation demonstrates a significant impact on the operation of the building. The penalty cost puts a limit on how much the operational cost increase for additional compensation should be, influencing the end CO_{2eq}-inventory. Increasing penalty costs decreases the end inventory, and a penalty cost of 10 $\frac{EUR}{kgCO_{2eq}}$ resulted in zero emission. The case achieving zero emission had an operational cost increase of 4.8% compared to operating without a penalty cost. This shows the importance of accounting for emissions during the operation of a ZEB, and the value of having an operational strategy that presents the future impact of operation.

1. Introduction

In the European Union (EU), buildings account for up to 80% of the total energy consumption [1]. Overall, the building stock amounts to 36% of the total CO_{2eq}-emissions in the EU [1].

1.1. Zero emission buildings

A considerable volume of research has been conducted on new solutions for Zero Emission Buildings (ZEBs) based on the definition from the Directive on Energy Performance of Buildings (EPBD) [2]. The Zero Emission Building research center[1] has explored how to increase the market penetration of buildings with low or net zero greenhouse gas (GHG) emissions over their lifetime [3]. The net zero emission goal considers the following phases of a building during its lifetime: construction, materials, operation, and end-of-life [4]. The critical phase for net zero emission is the operational phase, where emission compensation is required to cover the other phases [4]. In [5], the authors investigated existing definitions and calculation methodologies for ZEBs and zero energy buildings, identifying critical issues that should be addressed for a common ZEB definition and regulation. One specific issue identified concerned the period of calculating the energy and emission balance, where most methodologies presented used an annual balance.

As described and discussed in [6], the operational phase of a ZEB is affected by building location, energy sources in both the grid and on-site production, and the design choices for the buildings. It was observed that the emission compensation realized through the export of on-site renewable power generation depends on the electricity mix in the grid.

Most previous research on ZEBs uses annual average CO_{2eq}-intensities of the grid electricity. The authors in [7] optimized the design of a school building for different energy technologies, designed to be a zero energy building. In addition, emission compensation was included in the analysis through primal energy indicators for each technology. The results showed how the annual average CO_{2eq}-intensity

* Corresponding author.
E-mail address: kasper.e.thorvaldsen@ntnu.no (K.E. Thorvaldsen).
[1] https://www.zeb.no.

https://doi.org/10.1016/j.apenergy.2021.117415
Received 22 February 2021; Received in revised form 30 June 2021; Accepted 7 July 2021
Available online 12 August 2021

Nomenclature

Index sets

$\mathcal{T}$	Set of time steps within a week
G	Set of weeks within the year

Parameters

$\dot{E}^{B,dch}, \dot{E}^{B,ch}$	Discharge/charge capacity for battery [$\frac{\text{kWh}}{\text{h}}$]
$\dot{E}^{Max}$	Maximum EV charging capacity [$\frac{\text{kWh}}{\text{h}}$]
$\dot{Q}^{sh}$	Capacity for space heating radiator [$\frac{\text{kWh}}{\text{h}}$]
$\eta^{B}_{dch}, \eta^{B}_{ch}$	Discharge/charge efficiency for battery [%]
η^{EV}_{ch}	EV charging efficiency [%]
η^{PV}	Total efficiency for PV system [%]
C^{grid}	DSO energy tariff for imported energy [$\frac{\text{EUR}}{\text{kWh}}$]
$C^{\text{CO}_{2eq}}_{n}$	Expected future cost for point n [EUR]
$C_{\text{CO}_{2eq}}$	Penalty cost for negative end inventory at end of year [$\frac{\text{EUR}}{\text{kgCO}_{2eq}}$]
A^{PV}	PV system area [m^2]
C_i, C_e	Heat capacity for interior and building envelope [$\frac{\text{kWh}}{\text{°C}}$]
D^{EV}	EV discharge when not connected [kWh]
$E^{B,Cap}$	Battery storage capacity [kWh]
$E^{B,min}, E^{B,max}$	Battery SoC limits [kWh]
$E^{EV,Cap}$	EV storage capacity [kWh]
$E^{EV,min}, E^{EV,max}$	Min/Max EV SoC capacity [kWh]
$E^{0}_{\text{CO}_{2eq}}$	Initial accumulated CO_{2eq}-inventory [kgCO_{2eq}]
$E^{n,p}_{\text{CO}_{2eq}}$	Accumulated CO_{2eq}-inventory at point n [kgCO_{2eq}]
N_P	Number of discrete CO_{2eq}-inventory values
N_S	Number of nodes for stochastic variables
R_{ie}, R_{eo}	The thermal resistance between the interior-building envelope and building envelope-outdoor area [$\frac{\text{°C}}{\text{kWh}}$]
$T^{in,min}_t, T^{in,max}_t$	Lower/upper interior boundary [°C]
VAT	Value added tax for purchase of electricity [p.u]

Decision variables

$\alpha^{future}_{e_{\text{CO}_{2eq}}, s^s_{g+1}}$	Expected future cost from end accumulated CO_{2eq}-inventory [EUR]
γ	SOS-2 variables for the expected future cost curve
E^{B}_t	State of charge for battery at t [kWh]
E^{EV}_t	State of charge for EV at t [kWh]
$e_{\text{CO}_{2eq}}$	End accumulated CO_{2eq}-inventory at current decision stage [kgCO_{2eq}]
q^{sh}_t	Power usage for space heating at t [$\frac{\text{kWh}}{\text{h}}$]
T^{in}_t, T^{e}_t	Interior and building envelope temperature at t [°C]
$y^{B,ch}_t, y^{B,dch}_t$	Power to/from the battery at t [$\frac{\text{kWh}}{\text{h}}$]
$y^{EV,ch}_t$	Input power to EV at t [$\frac{\text{kWh}}{\text{h}}$]
y^{imp}_t, y^{exp}_t	Energy imported/exported at t [$\frac{\text{kWh}}{\text{h}}$]
y^{PV}_t	Power produced from PV system at t [$\frac{\text{kWh}}{\text{h}}$]

Stochastic variables

δ^{EV}_t	EV connected to building $\{0, 1\}$
C^{spot}_t	Electricity spot price at t [$\frac{\text{EUR}}{\text{kWh}}$]
D^{El}_t	Consumer-specific load at t [kWh]
$f^{\text{CO}_{2eq}}_t$	CO_{2eq}-intensity of electricity at t [$\frac{\text{kgCO}_{2eq}}{\text{kWh}}$]
I^{Irr}_t	Solar irradiation at building at t [$\frac{\text{kWh}}{\text{m}^2}$]
T^{out}_t	Outdoor temperature at t [°C]

from the grid affected the installation of energy carriers, based on net zero emission targets.

The work in [7] is extended in [8], comparing the use of hourly CO_{2eq}-intensities from the grid to yearly average for designing a Zero Emission Neighborhood (ZEN) in Norway. The findings showed that hourly emission intensity did not change the results significantly compared to using yearly average values.

In recent years there has been a development in the calculation of CO_{2eq}-intensities from the electrical grid. The authors in [9] calculated yearly average and marginal emission values for different zones in Europe based on future scenarios. In [10], average CO_{2eq}-intensities on an hourly resolution have been calculated for different bidding zones in Europe, by tracing the origin of electricity back to the generating unit. Similar work is presented in [11].

A building can be operated by a control system that adjusts flexible assets to shift their consumption. If the operation considers emission compensation, the CO_{2eq}-intensities can impact how the flexible resources are used. A yearly average CO_{2eq}-intensity offers no incentive for load shifting within the year, as the only focus for grid interaction lies in the net exchange over the year. With hourly average intensities, the timing of grid exchange within the year becomes more important. Use of flexible assets to adjust the grid interaction will provide short-term value for emission compensation. Moreover, hourly average intensities will promote import from the grid when the electricity mix in the grid has a low CO_{2eq}-intensity, i.e., has a higher share of renewable energy. Likewise, the export will be more favorable when there is a high CO_{2eq}-intensity in the grid. The definition in Norway regarding emission compensation for buildings uses time-dependent interaction [12], promoting operation considering the hourly CO_{2eq}-intensity as a means of achieving net zero emission.

1.2. Long-term building operation

In Norway, the optimal yearly strategy for emission compensation with hourly CO_{2eq}-intensity depends on the season. During winter, flexible assets can shift electricity import to time steps with lower CO_{2eq}-intensity, lowering inventory increase. During summer, local production can export electricity to reduce the CO_{2eq}-inventory. However, it is important to find a way of presenting the necessary contribution during the year, to reach the net zero emission goal. In addition, the uncertainty in operation needs to be accounted for. Uncertainty within load demand and local power production creates further uncertainty in the potential for emission compensation during the year. Providing the long-term impact of operational strategy is a vital tool for accurate performance when considering emission compensation, while including the uncertain impacts.

To the authors' knowledge, only a few studies consider the use of long-term price signals to optimize the short-term operation of buildings. However, this methodology is frequently applied to optimize the operation of other types of dispatchable assets in the power system, such as hydropower. Water values have been defined in hydropower scheduling to represent the future value of storing water in a reservoir, created through long-term scheduling models [13]. The generated

water values can be given as input for short-term scheduling models to consider the consequences of operation beyond the short-term horizon [14,15].

For long-term signals of buildings' operation, different clustering methods were tested in [16] for a ZEN over a year, finding the optimal design to achieve zero emission during operation. In [17], a stochastic dynamic programming (SDP) framework calculated and generated long-term price signals for the operation of a residential building. Future cost curves were generated to represent the change in future cost based on a measured-peak grid tariff (MPGT). The MPGT is a cost based on the highest single-hour peak import over a month. The future cost curves provided information about the full expected cost change for the future, balancing costs for increasing peak consumption and benefits from consumption adjustment with real-time pricing (RTP) costs. The same model was used in [18] to evaluate the individual value of flexibility from different flexible assets within the residential building using the same MPGT. The results showed the value of controlling flexible assets such as a stationary battery, electrical vehicle (EV) charging, and space heating (SH), and how the assets have different flexibility contributions.

The SDP framework from [17] could be implemented for the operation of a ZEB. However, the crucial point to enable this layout would be: How to tie emission compensation into the future cost curves? For the operation of a smart residential building, the overall goal is to minimize the total cost of operation. During operation of a ZEB, it is important to include both costs of operation and emission together, tying emission compensation into the objective function through a conversion factor, making the problem multi-objective. Some previous work has managed to combine the economic performance with emissions through multi-objective models. In [19], a planning framework for a local energy system is proposed, which included conversion factors for emission during operation. Emission reduction was focused upon when the authors in [20] wanted to look at how operating conditions for a cutting process could be tied to emissions, by using a conversion factor for emission based on carbon taxes.

The SDP framework can include the impact of emission compensation through the multi-objective layout, having the future cost curve based on both cost of operation and the penalty cost from net emission inventory. If disregarding the penalty cost for emission, the future cost only represents the expected cost of operation to minimize electricity cost over the year. Adding the penalty cost results in a future cost that co-optimizes operational cost and emission compensation. The SDP framework will generate curves throughout the year to highlight the penalty for emission at the end, generating a plan of operation to minimize the multi-objective cost while accounting for the seasonal variations and current point in time. The operational strategy generated could be given as input into a short-term operational model, so the long-term aspect of operation beyond the short-term horizon is included.

1.3. Our contribution

In this paper, we present a modified version of the SDP framework derived in [17], adjusted to capture the long-term economic impact of emission compensation for a ZEB during operation. The goal is to generate future cost curves showing the cost-optimal operational plan for achieving zero emission during building operation. The overall optimization model will be multi-objective, balancing both operational cost for electricity exchange and a penalty cost at the end of the year for remaining deviation from zero emission in the CO_{2eq}-inventory. Our contributions are the following:

- We include the future cost of emission compensation based on the current CO_{2eq}-inventory in building operation for a ZEB using SDP. The SDP framework defines an operational strategy throughout the year for cost-optimal emission compensation
- We investigate how the CO_{2eq} penalty cost for leftover CO_{2eq}-inventory puts an upper cost limit for emission compensation, and how a varying penalty cost changes the operational strategy throughout the year
- We look at how a finer resolution of the CO_{2eq}-intensity gives an added value to the use of flexible assets within the ZEB, where the flexible assets are controlled to increase emission compensation based on the variance in hourly CO_{2eq}-intensity

The remainder of the paper will be organized as follows: Section 2 describes the mathematical formulation of the multi-objective optimization model and the SDP framework. Section 3 will present the case study, while Section 4 presents and discusses the results and performance. Finally, a conclusion is given in Section 5.

2. Model description

The overall objective of the presented framework is to minimize the expected total operational cost of an all-electric residential building, while taking into account the cost of leftover CO_{2eq}-inventory at the end of the year. The horizon for this work is the course of a year and includes seasonal variation in emission compensation.

2.1. Model overview

A long-term operation model for a residential building is used to optimize the operational strategy of a ZEB over a one-year planning horizon. As mentioned in Section 1.2, the operating strategy acquired through the SDP framework can be used as input for a short-term operating model, to reach optimum long-term operation. The scheduling horizon depends on the long-term targets that the residential building is expected to reach. For instance, the MPGT investigated in [17] had a horizon of one month as the tariff was set based on the consumption over one month. The scope of this work considers a one-year horizon to capture the seasonal variations of CO_{2eq}-emissions. The problem is solved for weekly decision stages. For each week, the stochastic variables are known from the start of the week and throughout the week. This work considers the following stochastic variables: outdoor temperature, solar irradiation, electricity prices, hourly CO_{2eq}-intensity, consumer-specific load and EV availability.

Over the course of a year, we control the flexible assets within the building to adjust the import and export of electricity from the electricity grid in each week. The exchange of electricity directly impacts the CO_{2eq}-inventory, which is supposed to be net zero, otherwise a penalty should be paid for the leftover emission. The objective over the year is to minimize the total operating cost from the import and export of electricity, and the cost associated with the emission penalty:

$$min\mathbb{E}\{\sum_{t=1}^{8760}[C_t^{spot}\cdot(y_t^{imp}-y_t^{exp})+C^{grid}\cdot y_t^{imp}]+\Phi(e_{CO_{2eq}})\} \quad (1)$$

$\Phi(e_{CO_{2eq}})$ represents the cost for leftover accumulated emissions throughout the year. The inventory variable $e_{CO_{2eq}}$ keeps track of the emissions we receive during import of electricity from the grid, and the emissions compensated when exporting to the grid. A negative $e_{CO_{2eq}}$ inventory means that we have compensated more than we have acquired from import, while a positive inventory implies that we need to increase compensation to reach net zero emission at the end. The cost function for emission inventory is shown in Eq. (2), where we put a cost on having insufficiently compensated to reach our target emission inventory, X. Any extra emission compensated gives no further benefit, whereas any leftover emission results in a cost based on the leftover and the penalty cost $C_{CO_{2eq}}$.

$$\Phi(e_{CO_{2eq}})=\begin{cases}C_{CO_{2eq}}\cdot(e_{CO_{2eq}}-X), & \text{if } e_{CO_{2eq}}\geq X\\ 0, & \text{otherwise}\end{cases} \quad (2)$$

As the $e_{CO_{2eq}}$ is varying throughout the year and the initial value per week changes the strategy, this variable is coupled in time. With the time-coupling of the inventory, the optimization problem has a dynamic nature, making the overall problem in Eq. (1) a multi-stage stochastic optimization problem.

We apply SDP to solve the multi-stage stochastic optimization problem. With the use of dynamic programming, representing the expected future cost as a piecewise-linear cost curve, the overall problem can be decomposed into weekly deterministic subproblems. Each scenario per week comprises a unique subproblem to be solved. The SDP framework, further explained in Section 2.5, is solved in a backward procedure; we start at the last week of the year, and analyze backwards to the start of the year. With a backward procedure, we generate an operating strategy for each week that captures the future consequences, represented by expected future cost curves (EFCCs).

Using the SDP framework presented in [17] to find the optimal strategy for emission compensation allows us to decouple the year into multiple stages. Decoupling into stages decreases the complexity of each unique case that must be run. However, having too many stages or very high levels of detail in the future cost curves can lead to high run time. Another advantage of the SDP framework is the possibility to include uncertainty in the problem, which the clustering method from [16] did not include.

To enable coupling between the decision stages, we formulate a set $\mathcal{S}_g$ that contains information regarding everything that is carried over between decision stages. Within this set lies two subsets; $\mathcal{S}_{S,g}$ contains information on stochastic variables for the decision stage g, while $\mathcal{S}_{P,g}$ comprises the state variables in the optimization problem for formulating the future cost curve. The state variables comprise the discrete number of points for initial CO_{2eq}-inventory for each week that we investigate to find the change of the future cost curve with changing inventory values. The range of the discrete initial CO_{2eq}-inventories provides a good overview of what strategy one should implement during the year, both when the inventory is very negative or positive. Combined, a decomposed decision problem is defined by both subsets $s_g^s, s_g^p \in \mathcal{S}_g$, which indicates that, for a decision stage g, we analyze for a specific scenario and state variable for all combinations. State variables and the EFCC for each decision problem will be explained in Section 2.4.2, while the stochastic variables are described in Section 2.2.

2.2. Stochastic behavior

The stochastic scenarios that can occur throughout the year increase the complexity of the overall problem. In addition, uncertainty within weather has a serial correlation. This serial correlation makes it difficult to use a backward procedure, as history defines the current scenarios. To deal with the serial correlation, the scenarios are treated as a Markov decision process (MDP) using discrete states per scenario. The MDP assumes that scenarios are memoryless, meaning they have no information concerning how they got here, but do have information about their next scenario transition and the corresponding probabilities [21,22]. The MDP with the SDP framework makes the backward procedure possible. The coupling between the decision stages and scenarios is implemented as shown in Fig. 1, where a given scenario only contains and considers information on the future scenarios that can occur.

The scenarios represented in Fig. 1 are based on MDP behavior. For each decision stage, we have a finite number of discrete scenarios $s_g^s \in \mathcal{N}_S$ that can occur. Each of these scenario nodes contains values for the stochastic variables in the decomposed decision problem, each having a unique characteristic of the stochastic input. The transition probability $\rho(g, s_g^s | s_{g-1}^s)$ of transitioning from scenario node s_{g-1}^s to s_g^s during week $g-1$ to g is based on the probability function value between the two scenarios.

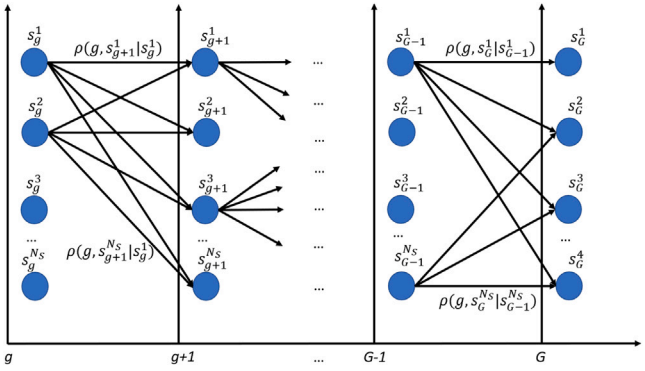

Fig. 1. Illustration of the scenario coupling between stage transition.

2.3. Decision stages

A given decision week g has an hourly time resolution. For each hour, the electricity demand must be met through exchange with the grid and the use of flexible assets to adjust consumption. At the start of each week, the electricity prices from the grid and all stochastic variables are assumed to be known. The flexible assets have identical start and end values on their energy levels for each decision stage, which for this problem includes a battery, EV, and indoor temperature. This simplification is introduced to ensure that the decision stage transition is feasible with equal values during transition, as their change in energy level and the corresponding future impact is not included in the future cost curve.

2.4. Decomposed decision problem

The decomposed decision problem is formulated as an optimization model for operating a ZEB with bi-directional power flow to the power grid. Different flexible assets are being controlled by the optimization model, so the flow of electricity within the building can be adjusted accordingly. The presented optimization model operates for a single deterministic stage of the overall SDP framework, for a given decision stage g, scenario s_g^s, and initial CO_{2eq}-inventory from the state variable s_g^p.

Within the building, there are several assets that the optimization model can control: a battery energy storage system (BESS), an EV charger, indoor space heating, and a roof-mounted photovoltaic (PV) system. Each flexible asset is modeled as a constraint-based asset, meaning they cannot operate outside of their given boundaries. The non-flexible electric-specific demand and heat demand for the water tank are assumed to be non-shiftable loads D_t^{El}, in which their demand must be met at all time steps.

2.4.1. Objective function

The objective function for the multi-objective problem is to minimize the total electricity cost for the end-user, while considering the expected future cost $\alpha^{future}_{e_{CO_{2eq}}, s^s_{g+1}}$ associated with the accumulated CO_{2eq}-inventory at the end of the stage. The cost is then tied to the time-dependent energy demand for the ZEB, RTP, CO_{2eq}-intensity over the stage, and the initial CO_{2eq}-inventory from the start of the week.

$$min\{\sum_{t\in\mathcal{T}}[C_t^{spot}\cdot(y_t^{imp}-y_t^{exp})+C^{grid}\cdot y_t^{imp}]+\alpha^{future}_{e_{CO_{2eq}}, s^s_{g+1}}\} \quad (3)$$

2.4.2. Emission compensation and future cost

The constraints regarding emission compensation and the setup for the expected future cost are presented in (4a) to (4e). The accumulated CO_{2eq}-inventory for this stage is showcased in (4a), where the accumulated inventory is based on the initial inventory value, and the sum of import and export with the time-dependent CO_{2eq}-intensities in the grid. The accumulated total sets the expected future cost variable $\alpha^{future}_{e_{CO_{2eq}},s^s_{g+1}}$ in (4b).

The $\alpha^{future}_{e_{CO_{2eq}},s^s_{g+1}}$ variable is set up using SOS-2 variables for the discrete values $E^{n,p}_{CO_{2eq}}$ $n \in \mathcal{N}_P$ to create a piecewise-linear cost curve based on the accumulated CO_{2eq}-inventory [23], named expected future cost curve (EFCC). The EFCC is made up of a number of discrete end CO_{2eq}-inventories, and a corresponding future cost based on the emission inventory, representing the expected future cost for the remaining period of the year. Uncertainty from future scenario nodes described in Fig. 1 is included, as the weighted cost is displayed in the EFCC. The EFCC is generated through the SDP framework, presented in Section 2.5.

$$e_{CO_{2eq}} = E^0_{CO_{2eq}} + \sum_{t\in\mathcal{T}} (y^{imp}_t - y^{exp}_t) \cdot f^{CO_{2eq}}_t \tag{4a}$$

$$\alpha^{future}_{e_{CO_{2eq}},s^s_{g+1}} = \sum_{n\in\mathcal{N}_P} \gamma_n \cdot C^{CO_{2eq}}_n \tag{4b}$$

$$e_{CO_{2eq}} = \sum_{n\in\mathcal{N}_P} \gamma_n \cdot E^{n,p}_{CO_{2eq}} \tag{4c}$$

$$\sum_{n\in\mathcal{N}_P} \gamma_n = 1 \tag{4d}$$

$$\gamma_n \geq 0 \quad \forall n,\ SOS\text{-}2 \tag{4e}$$

2.4.3. Energy balance

The energy balance for the electrical system in the building is given in (5). This includes import and export of electricity, local production from PV, charge and discharge from the BESS, load from SH and EV charging, and the non-elastic electrical demand.

$$y^{imp}_t - y^{exp}_t + y^{PV}_t + y^{B,dch}_t = D^{El}_t + y^{EV,ch}_t + q^{sh}_t + y^{B,ch}_t \quad \forall t \tag{5}$$

2.4.4. Electric vehicle

The EV system is formulated as shown in Eqs. (6a) to (6c). The EV has a uni-directional charging capability at a continuous rate, and availability for charging is given by the stochastic variable δ^{EV}_t. During time steps where it is not at the building, a constant discharge D^{EV} from the EV battery is occurring to simulate discharge from driving. The EV battery has a specified state-of-charge (SoC) range given in Eq. (6c), which is time-dependent to enable time-specific SoC preferences.

$$E^{EV}_t - E^{EV}_{t-1} = y^{EV,ch}_t \eta^{EV}_{ch} \delta^{EV}_t - D^{EV}(1-\delta^{EV}_t) \quad \forall t \tag{6a}$$

$$0 \leq y^{EV,ch}_t \leq \dot{E}^{Max} \quad \forall t \tag{6b}$$

$$E^{EV,min}_t \leq E^{EV}_t \leq E^{EV,max}_t \quad \forall t \tag{6c}$$

2.4.5. Battery energy storage system

The building has a bi-directional stationary battery available, which is controllable based on Eqs. (7a) to (7d). Power flow can be operated both ways at a continuous rate, where the limitation lies in power capacity and storage capacity. The storage capacity has a range to ensure optimal operation without damaging the battery.

$$E^B_t - E^B_{t-1} = y^{B,ch}_t \eta^B_{ch} - \frac{y^{B,dch}_t}{\eta^b_{dch}} \quad \forall t \tag{7a}$$

$$0 \leq y^{B,ch}_t \eta^B_{ch} \leq \dot{E}^{B,ch} \quad \forall t \tag{7b}$$

$$0 \leq y^{B,dch}_t \leq \dot{E}^{B,dch} \quad \forall t \tag{7c}$$

$$E^{B,min} \leq E^B_t \leq E^{B,max} \quad \forall t \tag{7d}$$

2.4.6. Photovoltaic system

A roof-mounted PV system is connected to the electrical system through a controllable system that allows the possibility to decrease power output if necessary.

$$0 \leq y^{PV}_t \leq A^{PV} \cdot \eta^{PV} \cdot I^{Irr}_t \quad \forall t \tag{8}$$

2.4.7. Space heating

SH of the building is formulated in (9a) to (9d). Heating of the building is done through an electric radiator with continuous output up to the rated capacity. Heat dynamics are represented as a grey-box model, so the physical behavior is formulated through linear state–space models [24,25].

The SH dynamics are presented as a 2R2C model, dividing the system into three thermal zones: the interior or indoor of the building, the envelope, and the outdoor area. The heat dynamics of the building are modeled without considering internal gains, solar gains or other heating gains except for a radiator. The control system can measure the interior, envelope and outdoor temperature, and operate the radiator to regulate the indoor temperature accordingly.

$$0 \leq q^{sh}_t \leq \dot{Q}^{sh} \quad \forall t \tag{9a}$$

$$T^{in,min}_t \leq T^{in}_t \leq T^{in,max}_t \quad \forall t \tag{9b}$$

$$T^{in}_t - T^{in}_{t-1} = \frac{1}{R_{ie}C_i}[T^e_{t-1} - T^{in}_{t-1}] + \frac{1}{C_i} q^{sh}_t \quad \forall t \tag{9c}$$

$$T^e_t - T^e_{t-1} = \frac{1}{R_{ie}C_e}[T^{in}_{t-1} - T^e_{t-1}] + \frac{1}{R_{eo}C_i}(T^{out}_{t-1} - T^e_{t-1}) \quad \forall t \tag{9d}$$

2.5. Solution strategy

Algorithm 1: The SDP algorithm to generate EFCCs per decision stage.

```
1 for g = G, G − 1, .., 1 do
2     for n ∈ N_P do
3         E^0_{CO2eq} ← E^{n,p}_{CO2eq}
4         for s^s_g ∈ N_S do
5             {C^spot_t, D^El_t, f^{CO2eq}_t, δ^EV_t, I^Irr_t, T^out_t} ← Γ(g, s^s_g)
6             C^{CO2eq}_i ← Φ(i, s^s_g, g + 1) for i = 1..N_P
7             C_{s^s_g,n} ← Optimize (3) − (9)
8         for s^s_{g−1} ∈ N_S do
9             Φ(n, s^s_{g−1}, g) = Σ_{s^s_g=1}^{N_S} C_{s^s_g,n} · ρ(g, s^s_g | s^s_{g−1})
```

To find the optimal strategy for minimizing electricity cost while performing emission compensation, the SDP algorithm showcased in Algorithm 1 is used in a backwards procedure, starting at the last stage of the horizon. The presented SDP algorithm will for every decision stage $g \in \mathcal{G}$, every discrete point of the state variable $n \in \mathcal{N}_P$, and every scenario $s^s_g \in \mathcal{N}_S$ optimize the decision problem described in Section 2.4 and calculate the economic performance. For each state of an initial CO_{2eq}-inventory and scenario given a decision stage g, we realize the stochastic variables with scenario-specific values from Γ in line 5. In line 6, the EFCC for the next decision stage $g+1$ is specified. For the initial case of $g = \mathcal{G}$, the EFCC is made up of a discrete number of states from Eq. (2). Using these values as input, the multi-objective problem is solved in line 7 to find the objective function value, which is the total cost from that stage and the expected future cost based on emission compensation.

As discussed earlier, transition between stages must be feasible. Therefore, the flexible assets and their energy levels T^{in}_t, T^e_t, E^{EV}_t and E^B_t, have a constant start/end condition that must be encompassed by the optimization problem. For SH, a high penalty cost is included for missing the target, but is not included in the EFCC calculation.

The objective function results in line 7 are part of what makes up the EFCC points $\Phi(n, s^e_{g-1}, g)$ for $n \in \mathcal{N}_P$. The EFCC values are calculated in lines 8–9, where each specific state variable point is derived. The future cost for a given state variable node n is calculated as the weighted future cost value for all scenarios that can occur in stage g, which will be representing this stage and state variable for stage $g-1$. The future cost connects stage $g-1$ to stage g, coupling the stage transition as shown in Fig. 1. We use the transition probabilities $\rho(g, s^s_g | s^s_{g-1})$ to find the weighted future cost based on the current scenario node from $g-1$. After finding the weighted future cost for each scenario and for all discrete state variables, the complete EFCC is calculated.

After calculating the EFCC for a given stage, the next stage $g-1$ is calculated with the new EFCCs as input for this stage, until arriving at the first stage of the problem. All the generated EFCCs provide an overview of the future cost with a change of operational strategy, capturing the long-term effects of emission compensation at the current time of the year.

3. Case study

The model presented has been applied to a residential building located in Southern Norway. This single-family house (SFH) has a control system for the flexible assets, and tracks the import and export of electricity and the corresponding hourly average CO_{2eq}-intensity in the grid. The period analyzed is the year 2017, with an hourly time resolution per week over 52 weeks and historical data making up the stochastic variables.

The SFH house is assumed to be part of a ZEN, and that only the community has any limitations on the export of electricity. The demand in the ZEN is assumed to be significant enough that our ZEB can export electricity to any neighboring building without causing any potential harm to the whole electricity system.

3.1. Building structure

3.1.1. PV system

The PV system on the roof has an installed capacity of 18.6 kW, which is connected to an MPP inverter with a combined constant conversion and MPP efficiency at 95% [26].

3.1.2. Inelastic consumer demand

The inelastic demand originates from two sources: The passive and user-specific electric-specific electricity consumption, and demand from passive domestic hot water (DHW) consumption. The DHW-consumption profile is based on the measurement of 49 water heaters at Norwegian households through the "Electric Demand Knowledge - ElDek"[2] research project by SINTEF Energy Research [27].

3.1.3. Heat dynamics

The heat dynamics of the building are represented as a single-room building with a 2R2C layout. The characteristics of the building are based on observed values from the Living Lab building built by FME ZEB and NTNU [28,29]. The Living Lab is a pilot project used to study various technologies and design strategies with the overall goal of reaching the zero emission target and analyzing thermo-physical properties [30]. Heating is performed through a 3 kW radiator which can operate continuously. The control system operates the radiator to keep the indoor temperature between 20–24 °C, based on the work in [31].

3.1.4. Stationary battery

The stationary battery is from SonnenBatterie [32] with a rated power input/output of 2.5 kW measured at the output of the inverter. The installed capacity is at 10 kWh, with a tolerated SoC set at between 10%–100% SoC. The round-trip efficiency is set to 85% from [33].

[2] https://www.sintef.no/prosjekter/eldek-electricity-demand-knowledge/.

3.1.5. Electric vehicle

A 24 kWh EV is selected for this study, with an operational range between 20%–90% of total capacity at all times. At departure, the SoC must be between 60%–90% as a countermeasure to range anxiety. The EV consumes electricity from the battery during the time it is offline to simulate driving. For each day, the EV is assumed to leave at 9 AM and arrive at 5 PM, which was found to be the expected departure/arrival time during weekdays for EVs in Norway [34], with an hourly average discharge rate at $D^{EV} = 1.08$ kWh. Moreover, the authors of [35] found small changes on arrival time between weekdays and weekends, and thus we assume the same departure/arrival time for the weekend.

3.1.6. Initial conditions

As mentioned in Section 2.5, the following variables have been given a start/end value to enable a feasible stage transition: $T^{in}_0 = 22$ °C, $T^e_0 = 20$ °C, $E^{EV}_0 = 14.4$ kWh, $E^B_0 = 5$ kWh.

3.1.7. Grid tariff cost

The residential building is assumed to have an energy-only grid tariff with the local DSO, in this case being Ringerikskraft [36]. The total volumetric cost for purchasing electricity in 2017 was at 0.03572 $\frac{\text{EUR}}{\text{kWh}}$ when including both the consumer energy cost and grid tariff cost, plus 25% VAT. The RTP cost of electricity comes in addition to this.

3.1.8. CO_{2eq}-intensity and electricity cost

This work has used hourly average CO_{2eq}-intensities acquired by the methodology presented in [10], to analyze the average intensities in a selection of bidding zones in NordPool. The method was extended to consider 36 bidding zones, and the input data were generalized to allow the possibility of acquiring data for multiple years. This work utilizes the average intensities for NO2 during the year 2017. The RTP used for the analysis are also for the year 2017 and NO2, acquired from NordPool [37].

3.2. Scenario generation

The control system together with the SDP algorithm allows the possibility for multiple input data to be uncertain in the period of operation. To limit the range of uncertainty, the work here considers uncertainty within weather effects, more specifically the outdoor temperature and solar irradiation. Information such as electricity price, CO_{2eq}-intensity, EV departure/arrival time, and electric-specific demand is considered deterministic for the year. Multiple scenarios in electricity price and CO_{2eq}-intensity would affect the EFFCs as they show the weighted future cost. For EV departure/arrival, different scenarios would influence the timing of charging. However, as found in [18], the EV has long periods where it can charge between traveling, and thus could more easily load-shift to more convenient time steps. Varying electric-specific demand scenarios would influence the total demand and need for compensation, and could lead to more need to peak-shave with the BESS in hours with higher CO_{2eq}-intensity.

In total, three scenarios per week have been generated. The three scenarios are based on a normal distribution of the weather effects, with the mean and standard deviation as the discrete scenarios. With a normal distribution, the probability distribution is at $\rho_\mu = 68.2\%, \rho_\sigma = 15.9\%$ for the three scenarios. The probability distribution for the future scenario nodes is the same regardless of the current operating scenario.

Data for the weather effects have been obtained from Renewables.ninja [38]. This website offers country-level data on an hourly time resolution for the period of 1980–2019 using the MERRA-2 tool [39], in which a population-weighted factor for the data was chosen for Norway. The historical data were then used to create hourly normal distributions on both outdoor temperature and solar irradiation, to generate three discrete scenarios per week, consisting of the mean and the standard deviation in both directions.

3.3. Model cases

The scope of this work is to investigate the operational strategy for a ZEB with a goal of achieving net zero emission. To achieve zero emission, a cost-optimal strategy regarding CO_{2eq}-inventory over the course of the year must be generated. Through generated EFCCs with the SDP framework, we find the cost-optimal strategy on emission compensation for each decision week. To obtain an accurate description of the EFCC, the state variables are made up of 400 discrete points, with step sizes of 1 $kgCO_{2eq}$ in the boundary −200 to 200 $kgCO_{2eq}$. With three scenarios and a total of 52 weeks, the total number of combinations to analyze amounts to 62,400 per case. In addition, we seek to analyze how the penalty cost for leftover emission plays a role in the operational strategy. The penalty cost will put an upper limit on the cost increase for emission compensation, and affect the end inventory at the end of the year. Therefore, the analysis will investigate the SDP framework for multiple penalty cost values. The penalty costs considered are between 0 and 10 $\frac{EUR}{kgCO_{2eq}}$. In comparison, the highest cost for CO_{2eq}-quotas in 2019 was at 0.029 $\frac{EUR}{kgCO_{2eq}}$ [40]. Putting a penalty cost up to 10 $\frac{EUR}{kgCO_{2eq}}$, will result in operation where net zero emission is the most crucial goal and electricity prices play a smaller role. Another work has explored a price interval for external compensation of CO_{2eq} between 0 to 2 $\frac{EUR}{kgCO_{2eq}}$ [8].

The impact of the penalty costs will be investigated in a simulation phase, where the economic performance over a year is analyzed week by week sequentially. We investigate the yearly performance 1000 times, each year with different scenario combinations. The initial start inventory is at 0 for each year.

In addition to the Norwegian case, we will compare the performance of this model and framework for the Danish bidding zone DK1. The comparison will provide a sensitivity analysis on how the strategy is influenced by location and temporal changes. For the Danish case, we have the same range of penalty costs, and a step size of 10 $kgCO_{2eq}$ between −1000 to 3000 $kgCO_{2eq}$. Input data for the weather are from the same source as for the Norwegian case, and the same regarding electricity and hourly CO_{2eq}-intensities, adjusted for the DK1 bidding zone.

4. Results & discussion

This section presents the results from the case study, and discusses the contributions and implications the results provide. As described in Section 2.5, the SDP framework generates expected future cost curves (EFCCs) for each stage during the course of a year. These curves represent the future costs for increased emission compensation, based on the CO_{2eq}-inventory. The future cost for compensation is influenced by the penalty cost at the end of the year, setting the threshold for how costly a marginal compensation increase should be. Either the compensation is performed through shifting load consumption, or it is dealt with at the end of the year as a penalty. Therefore, the penalty cost is crucial to the operational strategy throughout the year.

The results of the operational strategy from the EFCCs are presented in Section 4.1. Furthermore, the economic performance alongside net CO_{2eq}-inventory is found in Section 4.2, while the operational performance is showcased in Section 4.3. Finally, the performance for the Danish case study in DK1 will be investigated in Section 4.4.

4.1. Generation of expected future cost curves

The higher the penalty cost at the end of the year, the more the EFCC reflects the value of emission compensation throughout the year. Therefore, the future presents an opportunity to co-optimize operational cost and emission compensation. To illustrate the behavior of the curves over the whole year, and make them comparable, the EFCCs will be presented as marginal EFCCs (MEFCCs) in this section. The MEFCCs represent the marginal future cost of higher emission inventory, which is also the future cost saving if emission compensation is used to decrease the inventory marginally. Fig. 2 shows the MEFCCs for week 0 (which is the start of the year), for different penalty costs.

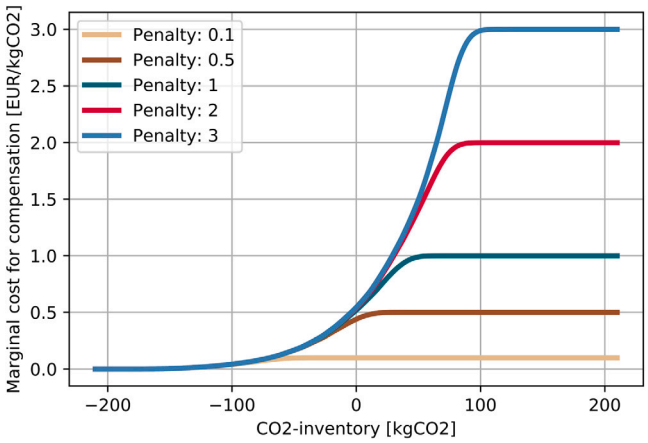

Fig. 2. MEFCCs for different penalty costs at week 0.

The MEFCCs in Fig. 2 capture how the future cost is affected by the change in CO_{2eq}-inventory, and that the inventory highly affects the marginal cost for emission compensation. On the far left of the figure, the marginal cost for inventory is 0. This 0 marginal cost is tied to the CO_{2eq}-inventory being at a satisfying level, where no future compensation that would increase cost of operation is needed to reach net zero emission. However, as the inventory increases, the net zero emission goal cannot be met without changing the operational strategy to include emission compensation during the year.

For a non-zero marginal value on the MEFCCs, the future cost portrays the expected future cost for the marginal CO_{2eq}-inventory increase. Some time in the future, there is a potential opportunity to increase compensation to decrease the inventory. This compensation opportunity and the corresponding cost are presented as this marginal cost, which we compare to the increased cost of increasing compensation at the current decision stage we are in. The optimization model finds the cost-optimal decision: Wait for the future, or adjust the operational plan now to increase compensation. For an increasing inventory, the marginal future cost increases, due to the increased emission compensation that is needed in the future for reaching net zero emission. Based on the current inventory, the MEFCC shows the highest marginal cost increase that should be considered for the decision stage.

The increase of marginal cost for the MEFCCs is tied to the penalty cost, which puts a limit on how much the marginal compensation increase should cost. As seen with the different penalty costs in Fig. 2, the future marginal cost flattens out at the penalty cost with increasing CO_{2eq}-inventory. This flat part represents the cost limit for compensation. If the marginal cost is equivalent to the penalty cost, increased compensation would reduce the penalty cost paid at the end. However, if the operational cost increase for decreasing the inventory is higher than the cost increase from the EFCCs, it is cost-wise better to pay the penalty at the end. Operating in the inventory level with a constant marginal cost indicates that the net zero emission goal will not be met, and that any further cost-optimal compensation increase only decreases the final penalty cost. Thus, the penalty cost influences our threshold for reaching zero emission. Note that the different MEFCCs start at the same point on the left side of the x-axis, but as the inventory increases, each one breaks off and flattens. The higher the penalty cost, the more cost-optimal opportunities exist, to cover the higher end cost. However, as the framework includes uncertainty, each MEFCC is a weighted future cost based on the weighted emission compensation in the future. The role of uncertainty is why the curves break off from the shared

path and slowly ascend towards the penalty cost; the weighted marginal cost is a combination of scenarios with different costs for compensation potential. Some scenarios would have cost-efficient compensation, and some scenarios find the specific penalty cost more cost-efficient.

The future marginal costs in the MEFCC in Fig. 2 present a future compensation opportunity that has not yet occurred. The boundary between marginal penalty cost and 0 decreases as the year progresses, due to fewer upcoming opportunities. This change in boundary means the curves also represent the range of how much the CO_{2eq}-inventory can vary while still achieving net zero emission at the end. Since the start of the year is plotted in Fig. 2, the boundary range shows the initial inventories we can start the year at to achieve zero emission without paying the penalty at the end. For a penalty cost above 0.5 $\frac{\text{EUR}}{\text{kgCO}_{2eq}}$, an initial CO_{2eq}-inventory at 0 or less should reach near zero emission without any penalty, although this is subject to uncertainty. Because of the potential for some penalty costs achieving zero emission even with a positive initial inventory level, the curves show the potential of covering embodied emission during operation.

As the MEFCCs are generated for each week during the year, the curves will change behavior to reflect the future potential given the weeks considered. Not only will the possible opportunities for compensation decrease as the year progresses, but the CO_{2eq}-inventory boundary between marginal penalty cost and 0 will shift on the x-axis. An inventory at 0 kgCO_{2eq} might be manageable at the beginning of the year for certain boundaries, but not necessarily possible without paying a penalty if we are in a later week. The seasonal variations for the MEFCCs are presented as heatmaps in Fig. 3 for four different penalty costs.

The heatmaps of the MEFCCs over the year capture the cost change in emission compensation, based on both the time of year and inventory. For a given curve, the change in where the marginal cost is between 0 and the penalty cost represents the seasonal variations. An increasing inventory during winter is expected from the figures due to high energy demand. The summer period expects high export to decrease the inventory again from, for example, high PV production. The seasonal variations of the inventory are present for all penalty costs. However, the penalty cost area is pushed up with increasing penalty cost, increasing the boundary where there exist future potential for compensation. With increasing penalty cost, more cost-optimal opportunities for compensation exists in the future, giving a broader range of acceptable inventory levels. If operating a ZEB to optimize cost while achieving zero emission, the MEFFCs show the range of acceptable inventory levels throughout the year to avoid paying the penalty cost.

4.2. Economic operational performance

The economic operational performance is investigated by computing a year sequentially week by week, which is performed 1000 times to account for uncertainty. The EFCCs are given as input to guide the model throughout the year to make cost-optimal decisions regarding emission compensation. Table 1 presents the yearly average total cost for the ZEB and the ending CO_{2eq}-inventory, for penalty costs between 0 and 10 $\frac{\text{EUR}}{\text{kgCO}_{2eq}}$.

The trend in Table 1 shows that an increasing penalty cost leads to increasing operating cost. Disregarding the penalty cost gives the lowest operating cost and highest ending CO_{2eq}-inventory, since only costs from grid interaction are prioritized. Increasing penalty cost leads to more focus on dealing with emission costs. The flexible assets change their consumption pattern to participate in emission inventory reduction through the indications from the EFCCs, increasing operational costs. In addition, the total cost when including the penalty cost also increases for increasing penalty costs. An increasing penalty cost taxes the ending inventory more, affecting total cost, and promoting reduction of inventory. The end inventory is decreasing for higher penalty cost, saturating towards 0 the higher the penalty cost. Starting at 0.5 $\frac{\text{EUR}}{\text{kgCO}_{2eq}}$, the penalty cost contributes to achieving an inventory close to 0, indicated by the decrease in penalty paid at the end of the year. This threshold indicates that the ZEB during operation on average is close to achieving net zero emission. The ending CO_{2eq}-inventory is plotted for the penalty costs as a boxplot in Fig. 4 to illustrate this behavior.

Table 1
Average total operating cost with/without the penalty cost, and average ending CO_{2eq}-inventory.

Penalty cost [$\frac{\text{EUR}}{\text{kgCO}_{2eq}}$]	Operating cost [EUR]	Operating cost + Penalty [EUR]	Ending CO_{2eq}-inventory [kgCO_{2eq}]
0	459.7	459.7	146.5
0.01	459.8	461.1	130.0
0.02931	460.2	463.4	108.5
0.05	460.8	465.4	92.1
0.1	462.7	469.4	66.5
0.2	466.6	474.6	40.1
0.5	477.2	480.2	6.0
0.75	479.7	480.9	1.7
1	480.5	481.2	0.71
2	481.3	481.5	0.090
3	481.5	481.6	0.029
10	481.7	481.8	0.0045

Fig. 4 shows the range of ending CO_{2eq}-inventory for the operation of a ZEB over a year, based on the penalty cost used. As the problem includes uncertainty, the end value is influenced by the scenarios realized, indicated by the spread of end inventory values for each case. For an increasing penalty cost, the inventory level decreases and slowly approaches net zero emission. From 1.0 $\frac{\text{EUR}}{\text{kgCO}_{2eq}}$, the expected range and both whiskers are close to zero emission. However, there are some few rare outliers present that affect the penalty at the end. The outliers decrease with increasing penalty, showing that higher penalty cost ensures more cases reaching net zero emission with operation throughout the year.

Looking at the spread of end CO_{2eq}-inventory in Fig. 4, it is first from a penalty cost of 0.5 $\frac{\text{EUR}}{\text{kgCO}_{2eq}}$ that the zero emission goal is achievable. The 0.5 $\frac{\text{EUR}}{\text{kgCO}_{2eq}}$ penalty cost has the lower whisker of the boxplot flattened around zero emission. This observation corresponds well with the details from Table 1, where the total cost increase started to flatten out at the same penalty cost. In addition, the same observation was made regarding the MEFCC for this penalty cost in Fig. 2. The figure showed that a start inventory at 0 could achieve zero emission for the 0.5 $\frac{\text{EUR}}{\text{kgCO}_{2eq}}$, since the marginal future cost was not equal to the penalty cost. However, as mentioned in Section 4.1, the uncertainty influences this interval, where some scenarios would have compensation opportunities, and some would result in a penalty paid at the end. This observation fits with how the boxplot for this penalty cost is represented in Fig. 4. For the favorable scenarios, the zero emission goal is within reach and the end inventory saturates at this level. However, the ill-favored scenario realizations lead to a range of inventory levels up to 25 kgCO_{2eq}.

Case $EL = 0$ in Fig. 4 ignores any consideration of electricity cost, only focusing on achieving zero emission during operation. This $EL = 0$ case shows that the ZEB is capable of achieving this goal if disregarding the cost of operation. When comparing to the cases with multi-objective focus, the output is similar to the highest penalty costs tested. For a penalty cost between 1–10 $\frac{\text{EUR}}{\text{kgCO}_{2eq}}$, the end inventory is close to zero emission while also accounting for ill-favored scenarios. From Table 1, the 10 $\frac{\text{EUR}}{\text{kgCO}_{2eq}}$ and 1 $\frac{\text{EUR}}{\text{kgCO}_{2eq}}$ penalty costs come at an operational cost increase of 4.8% and 4.5% compared to no penalty cost, respectively. The low cost increase difference between the two aforementioned penalty costs shows that the operational cost increase is not directly increasing in correspondence to the penalty cost. However, increasing penalty cost leads to fewer situations where one would risk a possible future scenario leading to an increased penalty at the end.

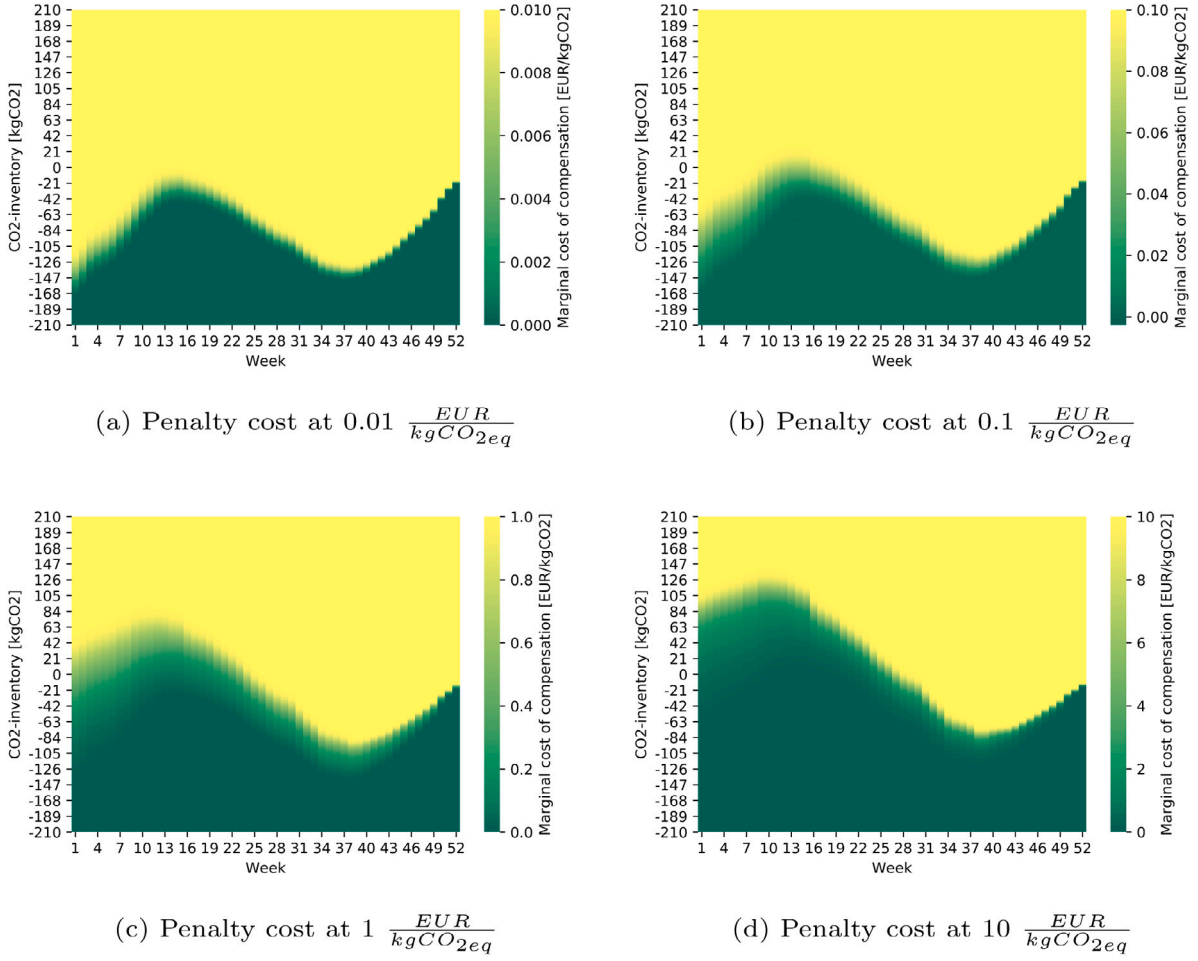

(a) Penalty cost at 0.01 $\frac{EUR}{kgCO_{2eq}}$

(b) Penalty cost at 0.1 $\frac{EUR}{kgCO_{2eq}}$

(c) Penalty cost at 1 $\frac{EUR}{kgCO_{2eq}}$

(d) Penalty cost at 10 $\frac{EUR}{kgCO_{2eq}}$

Fig. 3. Heatmap of the MEFCCs over a year with different penalty costs.

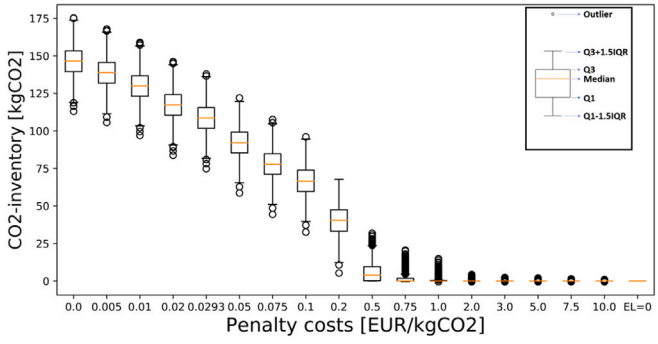

Fig. 4. Boxplot of the ending CO_{2eq}-inventory for the different penalty costs.

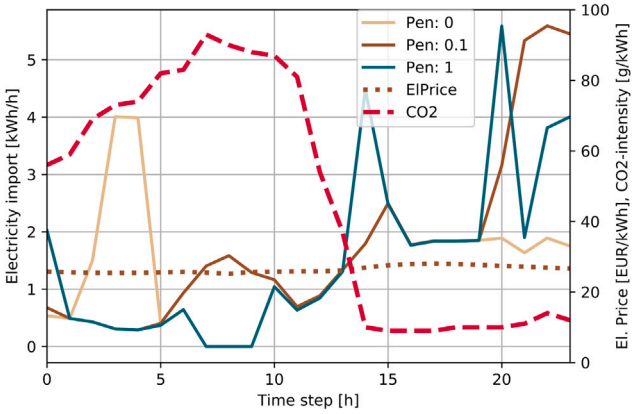

Fig. 5. The operational strategy during the first day for different penalty costs for a specific scenario. All cases have the same initial CO_{2eq}-inventory at start of operation.

4.3. Operation of the building

The operation of a ZEB will change based on the future implications given by the EFCC included as input. With an increasing penalty cost, the primary goal for the multi-objective optimization problem shifts to focus more on how to deal with the penalty cost at the end of the year. The EFCC changes the operational strategy regarding operational cost from grid interaction for the ZEB, shown in Fig. 5.

For the first day of the year 2017 in this analysis, as shown in Fig. 5, the grid interaction changes for a varying penalty cost. With a lower penalty cost, the operation focuses more on variation in electricity price, shifting electricity import more towards the night and afternoon where the electricity prices are normally lower. This strategy adjusts when the penalty cost increases, as the hourly CO_{2eq}-intensities have a different pattern than the electricity price for this day. With a higher intensity during the night and morning, the operational strategy for increasing penalty cost avoids high import of electricity for this period. In addition, there are periods where the import is lowered to 0 for the high penalty costs, which is to avoid high import of CO_{2eq} emission. The decrease of import causes a rebound effect later during the day,

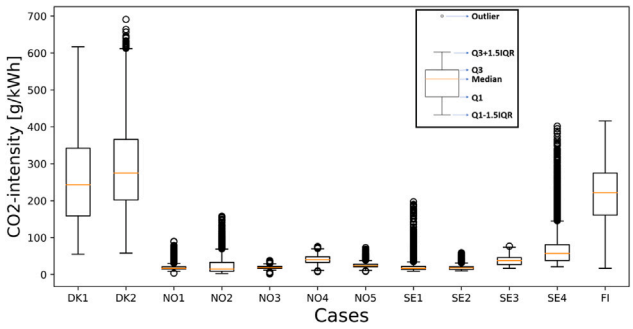

Fig. 6. Overview of hourly CO_{2eq}-intensities for the Nordic bidding zones in 2017.

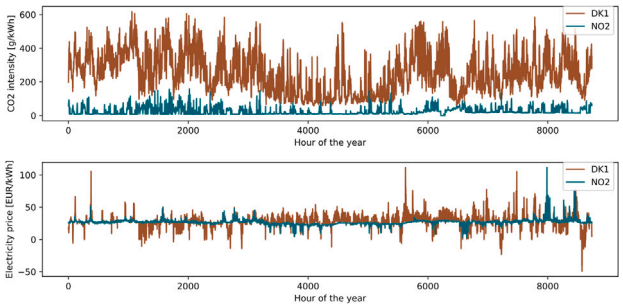

Fig. 7. Overview of hourly CO_{2eq}-intensities and electricity prices for DK1 and NO2 for the year 2017.

where the import increases with two high spikes during the evening for the 1 $\frac{\text{EUR}}{\text{kgCO}_{2eq}}$ penalty cost.

The operational strategy in Fig. 5 is during the first day of the year during winter. Periods of 0 import and high import spikes during the evening show an abnormal import strategy. This strategy indicates import during hours where there is increased risk of congestion in the grid. As discussed in [10], Norwegian bidding zones have tendencies where the electricity price and CO_{2eq}-intensity have opposite peaks during operation. The prices are low when the intensity is high and vice versa. This correlation is tied to the high amount of dispatchable hydropower sources available, which can store their water for production based on when the prices are highest, which then gives a high share of renewable energy when the electricity is needed the most. During hours with lower prices, the demand can be met with import from other bidding zones outside of Norway. NO2 is connected to both the Netherlands and Denmark, which when exporting to NO2 can give higher CO_{2eq}-intensity. Thus, this indicates that Norway with hydropower requires ZEBs to implement strategies that might go against a common strategy for the use of flexible assets, if hourly CO_{2eq}-intensities are to be used.

4.4. Comparison of emission compensation in DK1

Hourly average CO_{2eq}-intensity for bidding zones is tied together with the energy mix and interconnectors between each bidding zone. The energy mix is what not only comprises the CO_{2eq}-intensity on intensity levels, but also in the variation of intensity as some energy sources are intermittent and depend on the weather and other factors. The variations in the Nordic countries are shown in Fig. 6, where we see that both Norway and Sweden have the lowest intensity values. The intensity levels and variation in Norway are influenced by the high hydropower production [41]. For Denmark, the CO_{2eq}-intensity is higher and with more variation, due to a large amount of intermittent wind power and non-renewable energy sources [41]. Therefore, the value of operating a ZEB in DK1 and NO2 while considering emission compensation will have a different impact in each respective bidding zone. Not only will the variation in CO_{2eq}-intensity play an important role, but also how the variation is tied together with the electricity prices.

The Danish bidding zones experience more fluctuation in prices and CO_{2eq}-intensities than the Norwegian bidding zones for the year 2017, as shown in Fig. 7. NO2 shows lower variation and expected value of the CO_{2eq}-intensity over the year, from the high share of hydropower. DK1, with more intermittent wind power and interconnections to continental Europe, is more prone to both variation and higher intensity levels in its electricity mix. Denmark has a high proportion of wind power, but other energy sources with higher emission output are present, in addition to exchange with Germany and Norway. The variation in wind power output affects the average intensity during the year, and these variations would promote load shifting of a ZEB for emission compensation to a higher degree than the NO2 bidding zone can achieve.

The performance of the SDP framework for DK1 is presented in Fig. 8, where we include the MEFCC for different penalty costs at week 0, and a heatmap for the penalty cost of 0.1 $\frac{\text{EUR}}{\text{kgCO}_{2eq}}$. The main observation from both figures is the CO_{2eq}-inventory levels; a net zero emission goal for operation can be achieved without considering a penalty cost at all. The MEFCC has a 0 marginal cost at an initial inventory at 0 kgCO_{2eq} in both figures, showing that there is sufficient compensation when only considering cost of operation to achieve the emission goal. In addition, the MEFCC curve shows that there is high potential to increase compensation further, where one could have an initial value at 2000 kgCO_{2eq} with a penalty of 3 $\frac{\text{EUR}}{\text{kgCO}_{2eq}}$ and still be close to achieving zero emission. This high compensation potential is despite relatively lower CO_{2eq}-intensities during the summer period where there is high PV production compared to the rest of the year. The variation in CO_{2eq}-intensity promotes to a larger degree load shifting through flexible assets to increase compensation.

The economic performance for the different penalty costs ended on average with an inventory of −666 kgCO_{2eq} regardless of the penalty cost, which illustrates the zero emission goal is achieved with normal operation without emission penalty. The ZEB used for this case study has sufficient PV production, together with flexible assets, to adjust import and export of electricity to cost-optimal time periods, without considering the emission inventory. Fig. 9 presents the correlation between CO_{2eq}-intensity and electricity price for NO2 and DK1 over week 7 in 2017. Week 7 was chosen as it had varying CO_{2eq}-intensity and electricity prices in DK1 during late winter, where negative prices occurred for some hours.

For DK1 in Fig. 9, the correlation with intensity and price fits an operational strategy trying to minimize cost of operation; the intensity in the grid is high with high prices, and the intensity decreases more when the price decreases. Due to the intermittent wind production, more wind and lower intensity pushes the price down, favoring more consumption in terms of cost savings and emission inventory. For NO2, this trend is not shown, rather, the opposite trend is occurring more frequently due to the dispatchable hydropower. Therefore, operation in NO2 would require more change of operational strategy when considering emission inventory than for DK1. In addition, an operational strategy with an increasing focus on emission compensation would require higher operational costs for NO2 than for DK1. The observation shows that a ZEB with a zero emission goal is influenced to a greater extent by both the location, type of renewable generation in the electricity mix, and the temporal CO_{2eq}-intensity. The Danish case shows that with higher variation of CO_{2eq}-intensity, and correlation between electricity prices and CO_{2eq}-intensity, a ZEB is more capable of achieving net zero emission. In addition, the ZEB will have more capacity to deal with embodied emissions during operation, compensating for other phases during the ZEB's lifetime.

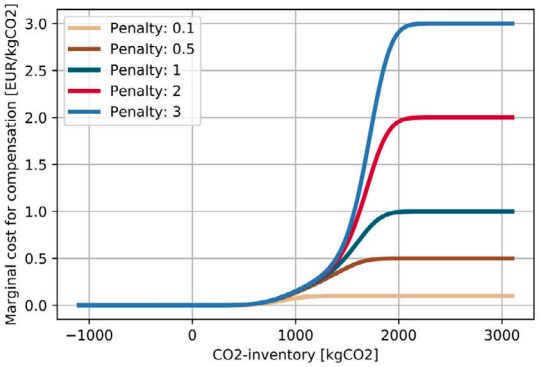

(a) MEFCCs for different penalty costs at week 0 for DK1.

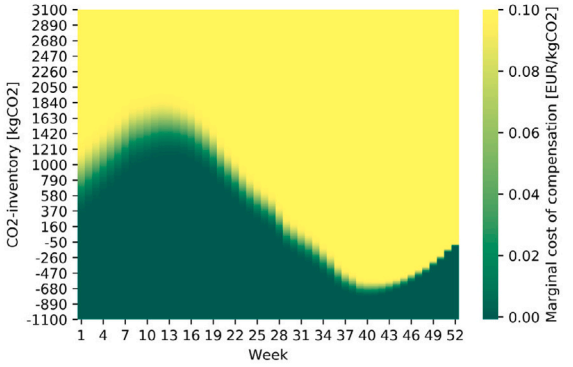

(b) Penalty cost at 0.1 $\frac{EUR}{kgCO_{2eq}}$ for DK1.

Fig. 8. Results of the SDP framework for DK1.

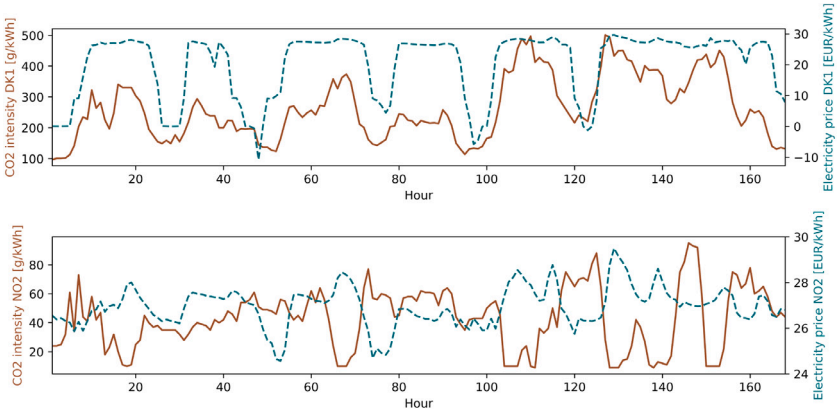

Fig. 9. Correlation between electricity prices and CO_{2eq}-intensities in NO2 and DK1 for week 7.

4.5. Limitations in this work

The work and results for the Danish and Norwegian cases have demonstrated the value of the optimization model and SDP-algorithm for building operation taking into account emission compensation. However, it is important to note the limitations of the presented approach, and what needs to be considered to implement this approach in practice.

Applications for automatic demand response with flexible assets are limited in real-world systems. Today, there exist pilot projects and local markets to promote end-user flexibility. However, they vary in different degrees depending on the regions and countries that the end-users are located in. In Norway, hourly electricity prices for end-users has been implemented through the roll-out of smart meters to residential and small business customers, while in France, flexibility markets for end-users are emerging and increasing in participation [42]. Enabling efficient market designs and price mechanisms for end-user flexibility is expected to increase the role of demand-side management on the end-user level in the future, which in turn can enable compensating CO_{2eq}-emissions from end-users.

Currently, real-time tracking CO_{2eq}-intensity and -inventory for end-users are not accounted completely during the power system operation. The power sector is primarily accounting for production-based emissions [11]. However, the consumer-based accounting methods, e.g., the proposed SDP-algorithm can assist end-users in tracking their emission impact over an operating year, based on both previous achievements and future compensation potential. This will particularly be relevant for Zero Emission Buildings and Neighborhoods, which has set clear long-term goals for the climate footprint: These users require operational tools to ensure that their day-to-day energy use is in line with the long-term goals.

5. Conclusion

Operating a zero emission building (ZEB) while accounting for both cost of operation and the hourly average grid CO_{2eq}-intensities over the course of a year requires the incorporation of a long-term strategy into the short-term operational decision-making process. Optimal operation of a ZEB requires accurate representation of both the CO_{2eq}-inventory to handle seasonal variations, and the cost-optimal time to use available flexible assets to increase emission compensation. We present a model that optimizes the operational strategy for emission compensation over a year, when trying to cost-optimally achieve zero emission for a ZEB during operation. Using a stochastic dynamic programming (SDP) framework, expected future cost curves (EFCCs) are generated, representing the future cost based on the current CO_{2eq}-inventory. The EFCC provides an overview of the marginal future value for increasing CO_{2eq}-compensation now versus later, throughout the year.

The proposed model was applied to a realistic Norwegian building located in the Norwegian bidding zone NO2 for the year 2017, to find the cost-optimal strategy for net zero emission. The operational strategy was tested for varying penalty costs at the end of the year. With an increasing penalty cost, the emission compensation increased, to counteract the penalty cost paid at the end. This is achieved by utilizing the available flexible assets in the ZEB to shift electricity import and export based on the variations in hourly average CO_{2eq}-intensity. A higher penalty cost made the flexible assets play a more

critical role, where they balanced the increased cost of operation to increase emission compensation against the future savings showed by the EFCCs. In addition, the temporal variation of the energy mix in different bidding zones impacts the operational strategy. DK1 showed a higher possibility of emission compensation, due to both higher variation in CO_{2eq}-intensity and better correlation between electricity prices and CO_{2eq}-intensity, compared to NO2.

When analyzing the economic performance over a year in NO2, the results showed that a penalty cost of 10 $\frac{\text{EUR}}{\text{kgCO}_{2eq}}$ met the net zero emission requirement at an expected total cost increase of 4.8% compared to not considering emission compensation. Without considering the emission compensation, the end CO_{2eq}-inventory was on average at 146.5 kgCO_{2eq}. Net zero emission was achievable from a penalty cost of 0.5 $\frac{\text{EUR}}{\text{kgCO}_{2eq}}$ and above. When increasing the penalty cost further, the average ending inventory reached closer to net zero emission and more cases reached zero emission, despite dealing with uncertainty during operation such as thermal demand and local production.

The operational strategy provided higher peaks of import with higher penalty costs, which could be at times when the electricity prices are high. With higher peaks at times with higher prices, this unnatural strategy could counteract congestion management, promoting further studies into how emission compensation can be performed from grid interaction. For instance, the introduction of marginal CO_{2eq}-intensities could be investigated. In addition, looking into embodied emissions for other phases during the lifetime of a ZEB would place more emphasis on the potential within the operational phase for compensation.

CRediT authorship contribution statement

Kasper Emil Thorvaldsen: Conceptualization, Data curation, Formal analysis, Investigation, Methodology, Software, Writing – original draft, Writing – review & editing. **Magnus Korpås:** Conceptualization, Formal analysis, Investigation, Methodology, Supervision, Writing – original draft. **Karen Byskov Lindberg:** Data curation, Formal analysis, Investigation, Supervision, Writing – review & editing. **Hossein Farahmand:** Data curation, Formal analysis, Investigation, Methodology, Supervision, Writing – original draft, Writing – review & editing.

Declaration of competing interest

The authors declare that they have no known competing financial interests or personal relationships that could have appeared to influence the work reported in this paper.

Acknowledgments

This work was funded and supported by the Research Council of Norway (Grant Number: 257626/257660/E20) and several partners through FME ZEN, Norway and FME CINELDI, Norway. The authors gratefully acknowledge the financial support from the Research Council of Norway and all partners in CINELDI and ZEN. In addition , special thanks to John Clauss for providing and helping with re-creating his methodology to generate hourly CO_{2eq}-intensity values. Finally, thank you to Linn Emelie Schäffer at NTNU for your valuable discussions and help in reviewing the manuscript.

References

[1] DIRECTIVE (EU) 2018/844 OF THE EUROPEAN PARLIAMENT AND OF THE COUNCIL of 30 May 2018 amending Directive 2010/31/EU on the energy performance of buildings and Directive 2012/27/EU on energy efficiency (Text with EEA relevance), Tech. rep., 2018.

[2] Directive 2010/31/EU of the European Parliament and of the Council of 19 May 2010 on the energy performance of buildings, Tech. rep., 2010.

[3] Lien K, Byskov Lindberg K. A Norwegian Zero Emission Building Definition, Tech. rep., URL http://www.laganbygg.se/UserFiles/Presentations/18._Session_5_T.Dokka.pdf, 2013.

[4] Selamawit F, Schlanbudch R, Sørnes K, Inman M, Andresen I. A norwegian ZEB definition guideline, Vol. January. 2016, p. 2017–24. http://dx.doi.org/10.13140/RG.2.2.26443.80162, URL.

[5] Marszal AJ, Heiselberg P, Bourrelle JS, Musall E, Voss K, Sartori I, Napolitano A. Zero energy building - a review of definitions and calculation methodologies. Energy Build 2011. http://dx.doi.org/10.1016/j.enbuild.2010.12.022.

[6] Fenner AE, Kibert CJ, Woo J, Morque S, Razkenari M, Hakim H, Lu X. The carbon footprint of buildings: A review of methodologies and applications. Renew Sustain Energy Rev 2018;94:1142–52. http://dx.doi.org/10.1016/J.RSER.2018.07.012, URL https://www.sciencedirect.com/science/article/pii/S1364032118305069.

[7] Lindberg KB, Doorman G, Fischer D, Korpås M, Ånestad A, Sartori I. Methodology for optimal energy system design of zero energy buildings using mixed-integer linear programming. Energy Build 2016;127:194–205. http://dx.doi.org/10.1016/j.enbuild.2016.05.039.

[8] Pinel D, Korpås M, B. Lindberg K. Impact of the CO2 factor of electricity and the external CO2 compensation price on zero emission neighborhoods' energy system design. Build Environ 2021;187:107418. http://dx.doi.org/10.1016/j.buildenv.2020.107418.

[9] Graabak I, Bakken BH, Feilberg N. Zero emission building and conversion factors between electricity consumption and emissions of greenhouse gases in a long term perspective. Environ Clim Technol 2014;13(1):12–9. http://dx.doi.org/10.2478/rtuect-2014-0002.

[10] Clauß J, Stinner S, Solli C, Lindberg K, Byskov, Madsen H, Georges L. General rights evaluation method for the hourly average CO2eq. intensity of the electricity mix and its application to the demand response of residential heating. 2019, http://dx.doi.org/10.3390/en12071345, Downloaded from Orbit.Dtu.Dk on.

[11] Tranberg B, Corradi O, Lajoie B, Gibon T, Staffell I, Andresen GB. Real-time carbon accounting method for the European electricity markets. Energy Strateg Rev 2019;26:100367. http://dx.doi.org/10.1016/j.esr.2019.100367.

[12] Norge S. Norsk Standard NS 3720:2018. Tech. rep., 2018.

[13] Helseth A, Fodstad M, Askeland M, Mo B, Nilsen OB, Pérez-Díaz JI, Chazarra M, Guisández I. Assessing hydropower operational profitability considering energy and reserve markets. IET Renew Power Gener 2017;11(13):1640–7. http://dx.doi.org/10.1049/iet-rpg.2017.0407.

[14] Fodstad M, Henden AL, Helseth A. Hydropower scheduling in day-ahead and balancing markets. In: International conference on the european energy market, EEM, Vol. 2015-August. IEEE Computer Society; 2015, http://dx.doi.org/10.1109/EEM.2015.7216726.

[15] Mo B, Fosso OB, Flatabø N, Haugstad A. Short-term and medium-term generation scheduling in the norwegian hydro system under a competitive power market. Tech. rep., 2002, URL https://www.researchgate.net/publication/306446062.

[16] Pinel D. Clustering methods assessment for investment in zero emission neighborhoods' energy system. Int J Electr Power Energy Syst 2020;121:106088. http://dx.doi.org/10.1016/j.ijepes.2020.106088.

[17] Emil Thorvaldsen K, Bjarghov S, Farahmand H. Representing long-term impact of residential building energy management using stochastic dynamic programming. In: 2020 international conference on probabilistic methods applied to power systems (PMAPS). IEEE; 2020, p. 1–7. http://dx.doi.org/10.1109/PMAPS47429.2020.9183623, URL https://ieeexplore.ieee.org/document/9183623/.

[18] Thorvaldsen KE, Korpås M, Farahmand H. Long-term value of flexibility from flexible assets in building operation. 2021, URL http://arxiv.org/abs/2105.11952.

[19] Botterud A, Holen AT, Catrinu M, Wolfgang O. Integrated energy distribution system planning: A multi-criteria approach optimal utilization of hydro power view project integrated energy distribution system planning: A multi-criteria approach. In: 15th power systems computation conference. Liege, Belgium; 2005, URL https://www.researchgate.net/publication/228340210.

[20] Liu ZJ, Sun DP, Lin CX, Zhao XQ, Yang Y. Multi-objective optimization of the operating conditions in a cutting process based on low carbon emission costs. J Cleaner Prod 2016;124:266–75. http://dx.doi.org/10.1016/j.jclepro.2016.02.087.

[21] Bellman R. A Markovian decision process -. 1957.

[22] Gudivada VN, Rao D, Raghavan VV. Big data driven natural language processing research and applications. In: Handbook of statistics, Vol. 33. Elsevier; 2015, p. 203–38. http://dx.doi.org/10.1016/B978-0-444-63492-4.00009-5.

[23] Beale EML, Forrest JJH. Global optimization using special ordered sets. Tech. rep., North-Holland Publishing Company; 1976, p. 52–69, URL https://link.springer.com/content/pdf/10.1007%2FBF01580653.pdf.

[24] Sonderegger RCRC. Dynamic models of house heating based on equivalent thermal parameters. PhDT 1978.

[25] Bacher P, Madsen H. Identifying suitable models for the heat dynamics of buildings. Energy Build 2011;43(7):1511–22. http://dx.doi.org/10.1016/j.enbuild.2011.02.005.

[26] Valentini M, Raducu A, Sera D, Teodorescu R. PV Inverter test setup for european efficiency, static and dynamic MPPT efficiency evaluation. In: 11th international conference on optimization of electrical and electronic equipment, OPTIM 2008. 2008, p. 433–8. http://dx.doi.org/10.1109/OPTIM.2008.4602445.

[27] SINTEF Energy Research KMB project 190780/S60, ElDeK, Electricity Demand Knowledge, URL https://www.sintef.no/en/projects/eldek-electricity-demand-knowledge/.

[28] ZEB Living Lab - https://www.zeb.no, URL https://www.zeb.no/index.php/en/pilot-projects/158-living-lab-trondheim.
[29] Vogler-Finck PJC, Clauß J, Georges L, Sartori I, Wisniewski R. Inverse Model Identification of the Thermal Dynamics of a Norwegian Zero Emission House. Springer, Cham; 2019, p. 533–43. http://dx.doi.org/10.1007/978-3-030-00662-4{_}44.
[30] Finocchiaro L, Goia F, Grynning S, Gustavsen A. The ZEB Living Lab: a multi-purpose experimental facility, Tech. rep., 2014.
[31] Berge M, Mathisen HM. Perceived and measured indoor climate conditions in high-performance residential buildings. Energy Build 2016;127:1057–73. http://dx.doi.org/10.1016/j.enbuild.2016.06.061.
[32] sonnenBatterie - https://sonnengroup.com, URL https://sonnengroup.com.
[33] Jafari M, Korpås M, Botterud A. Power system decarbonization: Impacts of energy storage duration and interannual renewables variability. Renew Energy 2020;156:1171–85. http://dx.doi.org/10.1016/j.renene.2020.04.144.
[34] Lakshmanan V, Bjarghov S, Olivella-Rosell P, Lloret-Gallego P, Munné-Collado I, Korpås M. Value of flexibility according to the perspective of distribution system operators — a case study with a real-life example for a Norwegian scenario, 2021.
[35] Sadeghianpourhamami N, Refa N, Strobbe M, Develder C. Quantitive analysis of electric vehicle flexibility: A data-driven approach. Int J Electr Power Energy Syst 2018;95:451–62. http://dx.doi.org/10.1016/j.ijepes.2017.09.007.
[36] Ringerikskraft - https://www.ringerikskraft.no/, URL https://www.ringerikskraft.no/.
[37] Nord Pool - https://www.nordpoolgroup.com, URL https://www.nordpoolgroup.com/.
[38] Renewables.ninja, URL https://www.renewables.ninja/.
[39] MERRA-2, URL https://gmao.gsfc.nasa.gov/reanalysis/MERRA-2/.
[40] CO2 European Emission Allowances PRICE Today — CO2 European Emission Allowances Spot Price Chart — Live Price of CO2 European Emission Allowances per Ounce — Markets Insider, URL https://markets.businessinsider.com/commodities/co2-european-emission-allowances.
[41] ORGANISATIONAL AND REGIONAL TABLES OECD Total, Tech. rep., URL www.iea.org/reports/covid-19-impact-on-electricity, 2021.
[42] Glover L, Villa M, Murley L, Coelho Ja, Adey-Johnson R, Pinto-Bello A. EU Market monitor for demand side flexibility. Tech. rep., 2021, URL www.delta-ee.com.